TITLE

A fusion of minicircle DNA and nanoparticle delivery technologies facilitates therapeutic genetic

engineering of autologous canine olfactory mucosal cells

AUTHOR LIST

Alexander M. Delaney,[‡a] Christopher F. Adams, [*‡a] Alinda R. Fernandes,[a] Arwa F. al-Shakli,[a] Jon

Sen,[b] Darren Carwardine,[c] Nicolas Granger[c] and Divya M. Chari[*a]

[a]Cellular and Neural Engineering Group, Institute for Science and Technology in Medicine, Keele

University, Keele, Staffordshire, ST5 5BG, UK.

E-mail: c.adams@keele.ac.uk; Tel: +44 (0)1782 733943

[b]Department of Neurosurgery, The Walton Centre for Neurology and Neurosurgery, Liverpool, L9

7BB, UK

[c]School of Veterinary Sciences, University of Bristol, Langford House, Langford, North Somerset

BS40 5DU, UK

[‡]These authors contributed equally to this publication.

ABSTRACT

Olfactory ensheathing cells (OECs) promote axonal regeneration and improve locomotor function when transplanted into the injured spinal cord. A recent clinical trial demonstrated improved motor function in domestic dogs with spinal injury following autologous OEC transplantation. Their utility in canines offers promise for human translation, as dogs are comparable to humans in terms of clinical management and genetic/environmental variation. Moreover, the autologous, minimally invasive derivation of OECs makes them viable for human spinal injury investigation. Genetic engineering of transplant populations may augment their therapeutic potential, but relies heavily on viral methods which have several drawbacks for clinical translation. We present here the first proof that magnetic particles deployed with applied magnetic fields and advanced DNA minicircle vectors can safely bioengineer OECs to secrete a key neurotrophic factor, with an efficiency approaching that of viral vectors. We suggest that our alternative approach offers high translational potential for the delivery of augmented clinical cell therapies.

INTRODUCTION

Spinal cord injury (SCI) can result in paralysis and reduction in patient quality of life, with high associated healthcare costs.[1] Transplantation of olfactory ensheathing cells (OECs) into sites of SCI has been identified in multiple pre-clinical studies as a potential regeneration promoting strategy;[2–5] offering high translational benefits due to ease of autologous cell derivation (using minimally invasive endoscopic surgery[6]). Crucially, a clinical trial in companion dogs with chronic naturally occurring thoracic SCI (e.g. degenerative disc prolapse) conducted in Cambridge in 2012, demonstrated improved locomotor recovery after transplantation of autologous nasal mucosa-derived OECs and fibroblasts versus controls.[7] This study is of significant interest for human applications as a large animal model of SCI, offering critical similarities to clinical SCI in humans in terms of lesion heterogeneity and pathogenesis. Indeed, safety trials since 2005 have established the therapeutic potential of OEC transplantation in human patients[8–11] and these have been accompanied by at least one high profile clinical case in Poland in which OEC transplantation into a site of complete spinal cord transection was followed by restoration of lower limb movement.[12]

However, improving the therapeutic capacity of OECs is a key clinical goal. For example, in the canine trial, secondary outcome measures including kinematic evaluation of brain controlled coordination did not indicate recovery of complex/brain-derived neurological functions.[7] Although the study was not powered to detect changes of these functions, it did not support evidence for long tract regeneration and restoration of cortical control. Genetic engineering of OECs for release of neurotrophic factors at injury sites offers a potential strategy for improved regenerative outcomes;[13,14] for example, OECs genetically modified to secrete neurotrophin-3 (NT-3) and glial cell line-derived neurotrophic factor (GDNF) show improved functionality post-transplantation versus non-engineered OECs.[15–17] Whilst work is ongoing to improve the safety of viral vector mediated bioengineering approaches, they can be associated with significant oncogenic[18] and inflammatory[19] risks to recipients. Along with safety issues, there are also challenges in pharmaceutical scale-up of viral engineering approaches,[20] meaning difficulties still remain in translating virally engineered OECs into the clinic.

As an alternative, we have previously shown that iron oxide magnetic particle (MP) vectors deployed with applied magnetic fields ('magnetofection') can safely engineer major rodent neural transplant populations including neural stem cells (NSCs) and oligodendrocyte precursor cells (OPCs).[21–23] MPs also offer key advantages in non-invasive transplant cell tracking in host tissue using standard neuroimaging technologies widely available within healthcare systems.[26] Optimizing MP based transfection procedures for transplant cells could therefore have critical importance with respect to MP mediated cell tracking if using appropriately designed particles (capable of transfection and MRI contrast generation).[27] This would be of high value to one-step combined transfection and tracking protocols for cell transplant populations, offering further benefits over other means of gene delivery. Further, the approach can be flexibly combined with advanced DNA minicircle (mC) vectors to safely deliver reporter/therapeutic genes to NSCs with similar efficiencies to viral vectors.[24,25] Despite the translational promise of this approach, application of this fusion of novel technologies to clinical cell populations has never been tested.

This study investigates the utility of the MP platform deployed with magnetic fields and mC DNA vectors for safe genetic engineering of canine OECs (cOECs), with a view to exploiting the technology in future canine transplantation trials. We have used banked cOECs derived for the Cambridge canine transplantation trial (which have pre-documented cellular characterisation and related records of clinical outcomes following transplantation). The aims of this proof of concept investigation were to: (i) develop optimised magnetofection protocols for gene delivery to cOECs using reporter plasmids; and (ii) use the optimised protocols to engineer cOECs to express a major neurotherapeutic protein-brain derived neurotrophic factor (BDNF) using mC vectors.

EXPERIMENTAL

Neuromag and mC complex characterization details

Neuromag is a commercially available transfection grade MP marketed by Oz Biosciences with a proprietary formulation. We have previously shown that the size of the naked MPs is ca. 300 nm (polydispersity index of 0.2) in DMEM which increases to ca. 900 nm (polydispersity index of 0.24) with the addition of the mC construct encoding BDNF.[25] The zeta potential of the resulting complex was shown to be 5.5 mV.[25] At the chosen ratio of 3.5 µL Neuromag to 1 µg DNA we have also shown that the entire DNA amount is associated with the particles.[28]

Primary canine olfactory mucosal cell (cOMC) culture

An OEC bank was generated during the clinical trial for OEC transplantation into sites of SCI in companion dogs[7] and used to generate the primary cOMCs used for all experiments. The cells were obtained as part of a protocol reviewed and approved by the Royal College of Veterinary Surgeons and the Ethical Review Committee of the Department of Veterinary Medicine, University of Cambridge. Details of recruitment and cell harvest methodology have previously been published.[7,29]

Magnetofection of cOMCs

Cells (passages 0–11) were seeded (1×10^5 cells per mL; 0.6 mL) on to PDL-coated coverslips in 24-well plates. After 24 h, the media in each well was replaced with fresh media (0.225 mL) and the plate returned to the incubator for a minimum of 2 h. To prepare nanoparticle complexes, 88 ng pmax-GFP was mixed with 0.31 µL Neuromag in 75 µL DMEM, corresponding to a Neuromag : DNA ratio of 3.5 µL µg−1. After 20 min, 75 µL complexes were added to each well (controls were DMEM alone) and plates were exposed to their respective magnetic field condition for 30 min. These were: no field, static field ($F = 0$ Hz), and oscillating fields of $F = 1$ Hz and F = 4 Hz. Control wells were not exposed to a magnetic field. Cells were then removed from the magnetic array and returned to the incubator for 24 h prior to fixing. To transfect cells with minicircles encoding BDNF (herein termed: mC-BDNF-GFP) the procedure was performed in an identical manner, using only a single optimum magnetic field condition and control.

mC vector formulation

The mC construct was prepared as previously described.[25] Briefly, 'parental plasmids' are transformed in ZYCY10P3S2T Producer Bacterial Strain, a specifically engineered *E. coli* strain which upon addition of arabinose express two enzymes: (i) ΦC31 integrase – which splits the parental plasmid into two circular entities, mC-DNA (size: 4.1 kb), and the bacterial backbone containing SceI endonuclease recognition sequence (size: 4.0 kb) and (ii) SceI endonuclease which degrades the bacterial backbone sequence. This leaves the mC-DNA which was extracted using an Endotoxin-free maxiprep kit (Qiagen, UK).

Analysis of MP uptake, transfection efficiency and safety of magnetofection

Cells were analysed at 24 h post transfection to assess transfection efficiency, particle uptake and measures of protocol safety. LIVE/DEAD staining was performed by incubating cells for 15 min in DMEM containing 4 μM calcein AM (green fluorescence in live cells) and 6 μM ethidium homodimer-1 (red fluorescence in dead cells). Remaining cells were fixed in 4% paraformaldehyde and stained with primary antibodies for p75 and Fn for Neuromag-GFP transfection and GFP and BDNF for mC-BDNF-GFP transfection. Merged fluorescent and phase images were used to estimate MP uptake, transfection efficiency and pyknotic nuclei. A Click-iT® EdU (a nucleoside analogue of thymidine incorporated in to DNA during active DNA synthesis) assay was performed to estimate numbers of proliferating cells by adding the EDU reagent 6 h prior to fixing and detection in fixed cells by fluorescent labelling. Immunostaining for copGFP (naturally occurring GFP with low fluorescence intensity) was used in the mC-BDNF-GFP experiments to enhance fluorescence for the purpose of cell counting. To assess transfection efficiency/success of the mC vector, cells were stained with primary antibodies for GFP and BDNF with GFP positive cells scored as transfected. Transfected cells were classified based on immunostaining and morphology and adapted from previous descriptions.[30] To determine the BDNF protein concentration in cell supernatants, an ELISA was applied using the Quantikine® ELISA Kit (R&D Systems, UK) according to the manufacturer's instructions.

Phase and fluorescence microscopy

Phase and fluorescence microscopy of all experiments was performed using an Axio Observer.Z1 equipped with an AxioCam MRm powered by Zen 2 (blue edition) software (Carl Zeiss MicroImaging GmbH, Goettingen, Germany). Images were merged and quantified using ImageJ 1.49v software.

Statistical analyses

For pmax-GFP transfection, all data were analysed by a one-way ANOVA with statistical differences determined by Bonferroni's multiple comparison test (MCT). For mC-BDNF-GFP transfection data were analysed using an unpaired t-test. In both cases, statistical differences were determined using Prism software (version 6.0). Data is expressed as mean ± standard error of the mean and the number of experiments 'n', refers to the number of independent cultures used. In this case, independent means different cell cultures each of which is derived from a different companion dog.

RESULTS

Field application enhances MP uptake and transfection efficiency in cOMCs

Primary cOMC populations were successfully recovered from frozen tissue banks and displayed normal morphologies and good adherence to the substrate (see ESI Fig. 1† for characterization). A 'safe' particle dose of 0.31 μL per well or 1.05 μL mL^{-1} was established here at which uniform cellular morphologies with no obvious rounding or detachment could be observed (Fig. 1A and B). Particles tended to be localised in the cell body, with almost no particles visible in cell processes (Fig. 1A and B). Under no field, the 'baseline' particle uptake was 86.0 ± 0.8% (range 85.0–87.2%; Fig. 1A and C), and significantly increased to 94.8% ± 1.6% when a static magnetic field was applied (range 91.8–99.3%; Fig. 1B and C). Application of oscillating fields significantly enhanced labelling versus no field but with no enhancement over the static field condition (Fig. 1C).

Expression of GFP was observed in all experimental conditions in both OEC and fibroblast-like cells, with uniform expression throughout transfected cells (Fig. 1D and E). Baseline transfection efficiency

in the no field condition was 34.9 ± 2.9% (range 28.8–42.7%; Fig. 1D and F) and increased to 57.7 ± 3.5% (range: 48.8–63.9%; Fig. 1E and F) in the static field condition. In line with particle uptake, application of oscillating magnetic fields significantly enhanced transfection over the no field condition but with no further improvements over the static field (Fig. 1F). Of the transfected cells across all conditions, 47.6 ± 3.1% displayed a bipolar fusiform morphology and p75 staining (classified as OECs); 29.3 ± 6.0% displayed fibroblast-like morphologies with strong Fn staining and 23.1 ± 3.5% could not be characterized phenotypically.

Magnetofection protocols had no effect on parameters of cell health

Magnetofected cultures displayed similar numbers of proliferating cells to control conditions, as measured by Click-iT® EdU proliferation assay, with GFP expressing cells also staining positive for the proliferation marker (Fig. 2A and D). Further, all conditions displayed similar and high viability (>95%) using a Live/Dead assay (Fig. 2B and E). Finally, the level of pyknosis (condensed and fragmented nuclei often a marker of cell death) was low and did not differ between experimental conditions, remaining below 2% in all conditions (Fig. 2C and F).

Rationale for selection of optimal magnetic field condition: delivery of mCs encoding BDNF

Overall, particle uptake and GFP expression did not differ significantly between conditions exposed to a magnetic field. Additionally, there was no evidence of differences in cellular viability and proliferation between experimental conditions. However, static magnets are considerably cheaper, do not require dedicated infrastructure, utilise technically facile protocols and are more readily available than oscillating magnetic arrays. As such, they have a greater practical relevance to magnetofection protocols performed in a clinical setting. Therefore, the static field was taken as the optimum field condition for transfection with mC-BDNF-GFP.

GFP staining successfully enhanced detection of GFP expressing cells (Fig. 3A) and transfection efficiency using mC-BDNF-GFP was estimated to be 8.1 ± 0.3% (range: 7.5–8.7%). Additionally, immunostaining for BDNF revealed a punctate pattern of fluorescence within GFP+ cells suggesting

intracellular vesicular storage of BDNF (Fig. 3B). There was also some weak BDNF staining visible within cells that did not express GFP (Fig. 3B), implying endogenous BDNF expression in cOMCs. However, mC-BDNF-GFP magnetofection resulted in a three-and-a-half-fold increase in the mean concentration of BDNF in cell supernatant versus controls (Fig. 3C) as determined by ELISA. Safety assays revealed that there were no significant differences between mC-BDNF-GFP transfected and untransfected control cells in terms of the percentage of proliferating cells, cell viability or percentage of pyknotic nuclei (Fig. 3D–F).

DISCUSSION

We demonstrate for the first time that non-viral MP based platforms in conjunction with magnetofection technology can safely and efficiently engineer cOMC populations, previously derived clinically for transplantation into dogs with SCI. Further, the approach could be combined with advanced mC-DNA vectors, which offer major translational advantages in terms of safety and enhanced gene expression, to successfully engineer cOMCs to secrete BDNF. We therefore suggest that these techniques may be adopted in future cOMC clinical trials in canines as an alternative to viral modification, a technique that has several regulatory hurdles preventing its widespread adoption.

Compared with previous reports, the transfection levels we have obtained for cOMCs appear to be within ranges reported for viral methods: Carwardine et al.[17] reported a maximum transduction efficiency of 34% at a multiplicity of infection (MOI) of 10, using chondroitinase ABC encoding lentiviral vectors and Ruitenberg et al.[31] reported 100% transduction of rodent olfactory bulb-derived OECs with a reporter plasmid at an MOI of 50 and 100 using lentiviral and adenoviral vectors, respectively. Wu et al.[32] transfected purified rodent olfactory bulb-derived OECs with a plasmid encoding NT-3 using a commercial lipofection agent, reporting a maximum transfection efficiency of 30% showing our techniques also compare favourably with other non-viral methods. It is worth noting that the cOMC transfection levels obtained with reporter plasmids are the highest we have achieved to date (in a transplant population for neurological applications) using magnetofection (Fig. 4), implying a high permissivity of this population to bioengineering approaches. High transfection

levels were achieved with a static field alone, whereas other cell types required application of specialized and expensive oscillating field equipment, offering further translational benefits.

Our ELISA analysis confirms that BDNF secretion from cOMC grafts could be enhanced threefold through MP mediated engineering approaches. BDNF is a key regenerative molecule and can promote local axonal sprouting and neuronal plasticity at CNS injury foci (reviewed by Weishaupt et al.[33]) indicating the potential to augment transplantmediated therapeutic capacity. Whilst BDNF secretion was markedly enhanced in engineered cells, the proportion of transfected cells was relatively low (ca. 8%). Two reasons could account for this: (i) a small number of cells secreting high levels of BDNF due to cellular heterogeneity in uptake of particle–plasmid complexes; or (ii) dissociation occurring at the transcription/translation level between the gene encoding BDNF and the downstream GFP gene – a well know issue with the internal ribosome entry site technology employed in the mC vectors.[34–36] If necessary, fluorescence-activated cell sorting could be utilized to purify transplant populations[37,38] in the future, in order to enhance the proportions of engineered cells in the grafts.

The mC technology used here offers several critical advantages for safe genetic engineering for clinical applications.[24,25] The removal of bacterial components found in conventional plasmids (including antibiotic resistance genes and an origin of replication) reduces numbers of unmethylated CpG motifs that can induce the host inflammatory response.[39] As such, regulatory bodies advise that use of antibiotic resistance genes should be limited where possible, particularly as their administration can limit other treatment options.[39–42] Absence of a bacterial backbone also mitigates gene silencing events, so mC technology can confer prolonged transgene expression versus conventional plasmids.[24] Additionally, the relatively small size of mCs (1.6 kb) could allow for incorporation of therapeutic genes such as that encoding chondroitinase ABC (insert size: 2 kb), without significantly reducing transfection efficiency. Additional neurotrophic genes (typical open reading frames of 1.2 kb) could also be inserted in place of the GFP reporter sequence (size ca. 756 bp), without appreciably increasing construct size. It is noteworthy that in light of the clinical utility of mC constructs, a novel method of obtaining highly purified mC-DNA for clinical applications such as gene therapy and

vaccination has been developed involving affinity based chromatography, which enables safe production of mCs at an industrial scale.[43–45]

CONCLUSION/FUTURE DIRECTIONS

We have demonstrated that mixed cOMC populations can be engineered to serve as biopumps for delivery of neurotherapeutic factors. In the context of developing a safe and effective therapy for SCI, we consider that the combination of advanced methodologies utilised here offers several clinical translational advantages. OECs are a promising clinical population due to their relatively straightforward autologous derivation and their proven potential in promoting repair after SCI. Further, engineering OECs using the MP platform and advanced mC vector technology seems particularly advantageous given the efficient particle uptake by OECs and the lack of detectable effects on cell health. This means that the additional benefits provided by the MP platform, such as the use of bimodal nanoparticles for simultaneous gene delivery and imaging[27] could be safely exploited. Future work will deploy this therapy in vivo in clinical spinal injuries (including in canine trials), and explore the ability of this technical approach to deliver other genes involved in repair such as additional neurotherapeutic factors to promote growth, chondroitinase ABC to degrade the glial scar,[17,46] and VEGF to promote local angiogenesis.[47]

REFERENCES

1. Spinal-research.org, 2016.

2. Y. Li, P. M. Field and G. Raisman, *Science*, 1997, 277, 2000–2002.

3. Y. Li, P. M. Field and G. Raisman, *J. Neurosci.,* 1998, 18, 10514–10524.

4. A. Ramón-Cueto, M. I. Cordero, F. F. Santos-Benito and J. Avila, *Neuron*, 2000, 25, 425–435.

5. N. Granger, R. J. M. Franklin and N. D. Jeffery, *Neuroscientist*, 2014, 20, 623–638.

6. P. J. Andrews, A.-L. Poirrier, V. J. Lund and D. Choi, *Rhinology*, 2016, 54, 183–191.

7. N. Granger, H. Blamires, R. J. M. Franklin and N. D. Jeffery, *Brain*, 2012, 135, 3227–3237.

8. F. Féron, C. Perry, J. Cochrane, P. Licina, A. Nowitzke, S. Urquhart, T. Geraghty and A. Mackay-Sim, *Brain*, 2005, 128, 2951–2960.

9. A. Mackay-Sim, F. Feron, J. Cochrane, L. Bassingthwaighte, C. Bayliss, W. Davies, P. Fronek, C. Gray, G. Kerr, P. Licina, A. Nowitzke, C. Perry, P. A. S. Silburn, S. Urquhart and T. Geraghty, *Brain*, 2008, 131, 2376–2386.

10. H. S. Chhabra, C. B. Lima, S. C. Sachdeva, A. D. Mittal, V. A. Nigam, D. E. Chaturvedi, M. Arora, A. H. Aggarwal, R. I. Kapur and T. A. H. Khan, *Spinal Cord*, 2009, 47, 887–895.

11. C. Lima, P. Escada, J. Pratas-Vital, C. Branco, C. A. Arcangeli, G. Lazzeri, C. A. S. Maia, C. Capucho, A. Hasse-Ferreira and J. D. Peduzzi, Neurorehabil. *Neural Repair*, 2010, 24, 10–22.

12. P. Tabakow, G. Raisman, W. Fortuna, M. Czyz, J. Huber, D. Li, P. Szewczyk, S. Okurowski, R. Miedzybrodzki, B. Czapiga, B. Salomon, A. Halon, Y. Li, J. Lipiec, A. Kulczyk and W. Jarmundowicz, *Cell Transplant*., 2014, 23, 1631–1655.

13. S. Thuret, L. D. F. Moon and F. H. Gage, *Nat. Rev. Neurosci*., 2006, 7, 628–643.

14. M. B. Bunge, *J. Spinal Cord Med*., 2008, 31, 262–269.

15. L. Cao, L. Liu, Z.-Y. Chen, L.-M. Wang, J.-L. Ye, H.-Y. Qiu, C.-L. Lu and C. He, *Brain,* 2004, 127, 535–549.

16. M. J. Ruitenberg, D. B. Levison, S. V. Lee, J. Verhaagen, A. R. Harvey and G. W. Plant, *Brain*, 2005, 128, 839–853.

17. D. Carwardine, L.-F. Wong, J. W. Fawcett, E. M. Muir and N. Granger, *J. Neurol. Sci.*, 2016, 367, 311–318.

18. M. Rothe, U. Modlich and A. Schambach, Curr. *Gene Ther*., 2013, 13, 453–468.

19. M. A. Witlox, M. L. Lamfers, P. I. J. M. Wuisman, D. T. Curiel and G. P. Siegal, *Bone*, 2007, 40, 797–812.

20. M. Elsabahy, A. Nazarali and M. Foldvari, Curr. *Drug Delivery*, 2011, 8, 235–244.

21. M. R. Pickard and D. M. Chari, *Int. J. Mol. Sci.*, 2010, 11, 967–981.

22. S. I. Jenkins, M. R. Pickard, N. Granger and D. M. Chari, *ACS Nano*, 2011, 5, 6527–6538.

23. M. R. Pickard, C. F. Adams, P. Barraud and D. M. Chari, *J. Funct. Biomater.*, 2015, 6, 259–276.

24. A. R. Fernandes and D. M. Chari, *J. Controlled Release*, 2016, 238, 289–299.

25. A. R. Fernandes and D. M. Chari, *J. Controlled Release*, 2016, 238, 300–310.

26. N. Panagiotopoulos, R. L. Duschka, M. Ahlborg, G. Bringout, C. Debbeler, M. Graeser, C. Kaethner, K. Lüdtke-Buzug, H. Medimagh, J. Stelzner, T. M. Buzug, J. Barkhausen, F. M. Vogt and J. Haegele, *Int. J. Nanomed*., 2015, 10, 3097–3114.

27. C. Adams, L. L. Israel, S. Ostrovsky, A. Taylor, H. Poptani, J.-P. Lellouche and D. Chari, *Adv. Healthcare Mater*., 2016, 5, 841–849.

28. M. R. Pickard and D. M. Chari, *Nanomedicine*, 2010, 5, 217–232.

29. N. D. Jeffery, A. Lakatos and R. J. M. Franklin, *J. Neurotrauma*, 2005, 22, 1282–1293.

30. K. Gladwin and D. Choi, *World Neurosurg*., 2015, 83, 114–119.

31. M. Ruitenberg, G. Plant, C. Christensen, B. Blits, S. Niclou, A. Harvey, G. Boer and *J. Verhaagen, Gene Ther*., 2002, 9, 135–146.

32. J. Wu, T.-S. Sun, J.-X. Ren and X.-Z. Wang, *Neurosci. Bull.*, 2008, 24, 57–65.

33. N. Weishaupt, A. Blesch and K. Fouad, *Exp. Neurol.*, 2012, 238, 254–264.

34. Y. Zhou, J. Aran, M. M. Gottesman and I. Pastan, Hum. *Gene Ther*., 1998, 9, 287–293.

35. L. M. Houdebine and J. Attal, *Transgenic Res.*, 1999, 8, 157–177.

36. H. Bouabe, R. Fässler and J. Heesemann, *Nucleic Acids Res.*, 2008, 36, e28.

37. C. A. Gorrie, I. Hayward, N. Cameron, G. Kailainathan, N. Nandapalan, R. Sutharsan, J. Wang, A. Mackay-Sim and P. M. E. Waite, *Brain Res.*, 2010, 1337, 8–20.

38. L. N. Novikova, S. Lobov, M. Wiberg and L. N. Novikov, *Exp. Neurol.*, 2011, 229, 132–142.

39. P. Mayrhofer, M. Schleef and W. Jechlinger, *Methods Mol. Biol.*, 2009, 542, 87–104.

40. A. M. Darquet, B. Cameron, P. Wils, D. Scherman and J. Crouzet, *Gene Ther*., 1997, 4, 1341–1349.

41. Z. Chen, C.-Y. He, A. Ehrhardt and M. A. Kay, *Mol. Ther.*, 2003, 8, 495–500.

42. L. E. Gracey Maniar, J. M. Maniar, Z.-Y. Chen, J. Lu, A. Z. Fire and M. A. Kay, *Mol. Ther.*, 2013, 21, 131–138.

43. P. Mayrhofer, M. Blaesen, M. Schleef and W. Jechlinger, *J. Gene Med.*, 2008, 10, 1253–1269.

44. M. A. Kay, C.-Y. He and Z.-Y. Chen, *Nat. Biotechnol.*, 2010, 28, 1287–1289.

45. D. Kobelt, M. Schleef, M. Schmeer, J. Aumann, P. M. Schlag and W. Walther, *Mol. Biotechnol.*, 2013, 53, 80–89.

46. E. J. Bradbury, L. D. F. Moon, R. J. Popat, V. R. King, G. S. Bennett, P. N. Patel, J. W. Fawcett and S. B. McMahon, *Nature*, 2002, 416, 636–640.

47. H. M. Kim, D. H. Hwang, J. E. Lee, S. U. Kim and B. G. Kim, *PLoS One*, 2009, 4, e4987.

FIGURES

Figure 1 : Magnetic field application increases particle uptake and transfection efficiency. (A&B) Representative fluorescent/phase images showing fluorescent Neuromag uptake in the (A) no field and (B) static field condition. (A-inset) Representative fluorescent/phase image showing abnormal cellular morphologies when magnetofection was attempted with 2.1 μL mL^{-1} Neuromag. Note cell rounding, retraction of processes and detachment. Scale bar in inset is 25 μm. (C) Graph showing quantification of the proportions of cells which displayed nanoparticle uptake. (D&E) GFP expression in (D) no field and (E) static field conditions with GFP+ fibroblasts depicted in the insets. (F) Graph showing quantification of the proportion of transfected cells in each field condition. **$P < 0.01$ versus no field. $n = 4$, one-way ANOVA and Bonferroni's MCT. NF – no field.
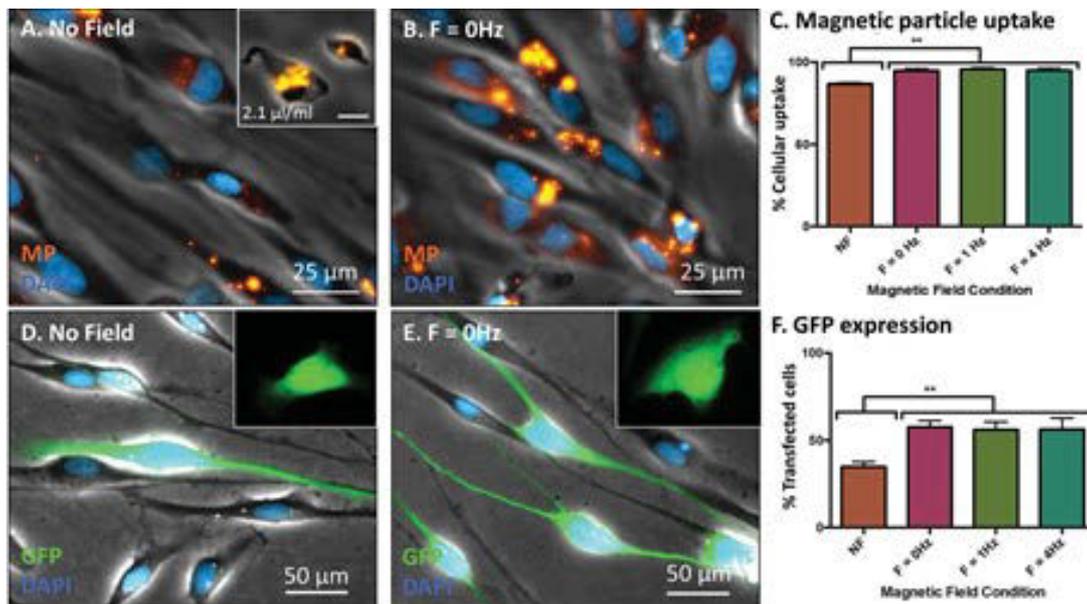
Figure 2. Cellular viability and proliferation were unaffected by magnetofection protocols. (A) Representative double merged fluorescent image of EdU+ GFP+ cells in the static field condition. Two adjacent, transfected EdU+ cells (arrow) suggest recent division. (B) Representative double merged image of Live/Dead staining in the static field condition showing high numbers of live (green) cells with a small proportion of dead (red) cells (arrow). (C) Representative fluorescent and phase merged image of a cell displaying typical pyknotic nuclei with condensation and nuclear fragmentation. (D–F) Graphs showing quantification of (D) the percentage of cells positive for EdU, (E) the percentage of live cells and (F) the percentage of cells which displayed pyknotic characteristics across all conditions. $n = 4$. NF – no field.
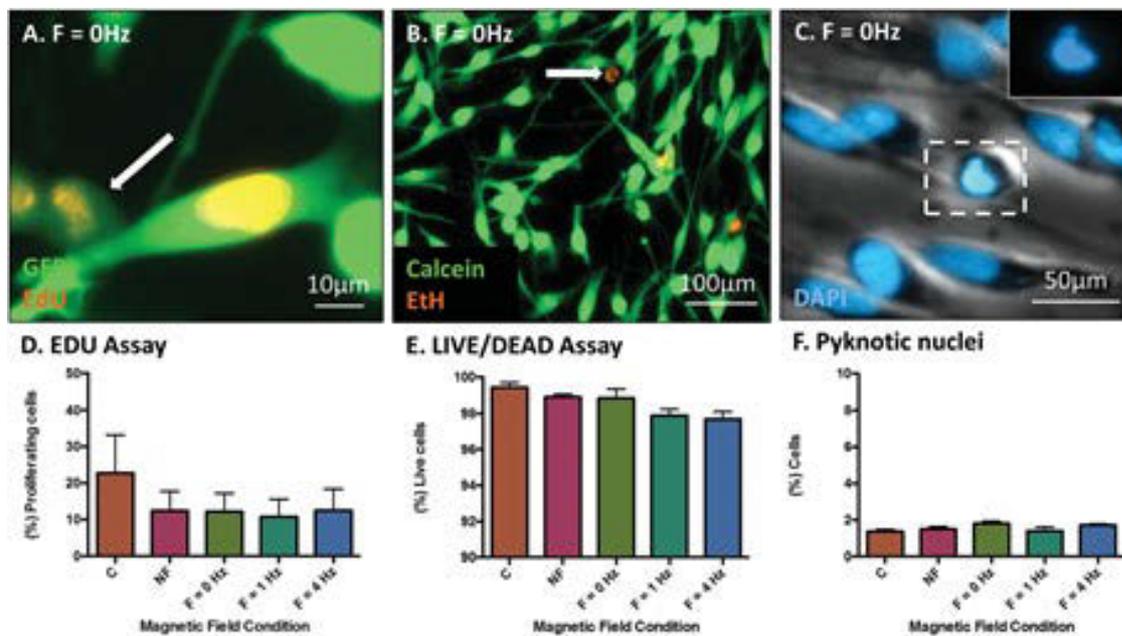
Figure 3. MPs can effectively deliver mC-BDNF-GFP to cOMCs, with no effect on cellular viability or proliferation. (A) Representative fluorescent images showing GFP staining enhances copGFP fluorescence (inset). (B) Representative triple merged fluorescent image showing BDNF accumulation inside transfected cells (inset – counterpart double merged image just showing BDNF staining). Note small quantities of BDNF inside adjacent untransfected cell. (C) Graph showing concentration of BDNF in cOMC culture supernatant in both conditions. (D–F) Graphs showing quantification of (D) percentage of cells positive for EdU, (E) percentage of live cells and (F) percentage of cells which displayed pyknotic characteristics across both conditions. *$p < 0.05$ versus control, unpaired t-test, $n = 3$.
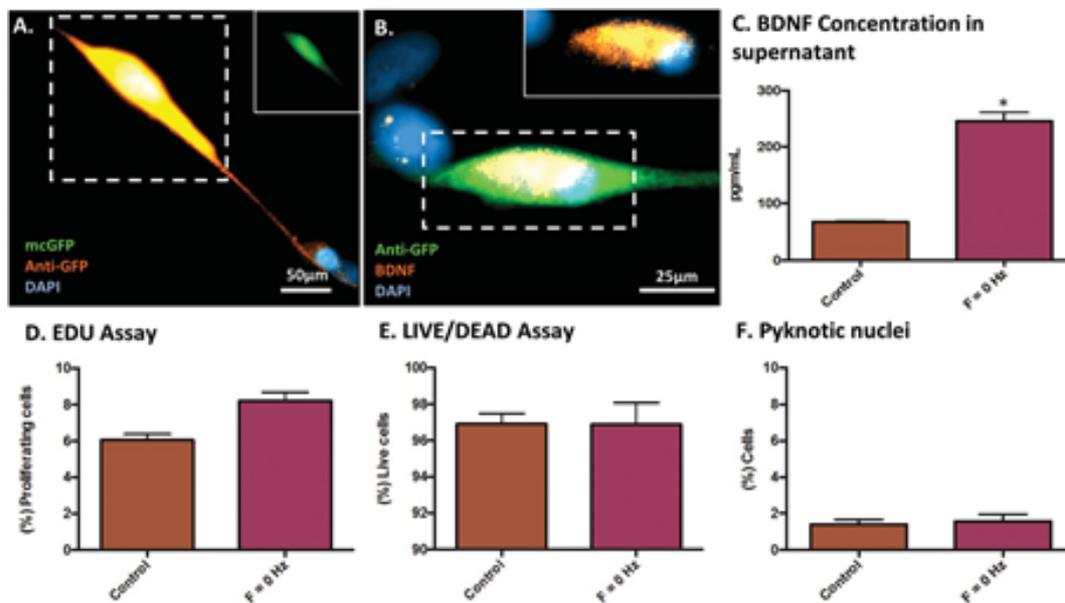
Figure 4. cOMCs show a greater permissiveness for transfection than NSCs and OPCs. Graph displaying how transfection efficiency in cOMCs compares to that seen in other neural cell populations for which we have developed optimised magnetofection protocols. Adapted from ref. 22, 23, 31 and 32.